Connecting Interfacial Mechanical Adhesion, Efficiency, and Operational-Stability in High-Performance Inverted Perovskite Solar Cells

Zhenghong Dai [1,9], Shuai You [2,9], Dwaipayan Chakraborty [1], Shunran Li [3,4], Yadong Zhang [5], Anush Ranka [1], Stephen Barlow [5], Joseph J. Berry [5,6,7], Seth R. Marder [5,6,8], Peijun Guo [3,4], Yue Qi [1], Kai Zhu [2,*], and Nitin P. Padture[1,*]

[1] School of Engineering, Brown University Providence RI 02912, USA

[2] Chemistry and Nanoscience Center, National Renewable Energy Laboratory, Golden, CO 80401, USA

[3] Department of Chemical and Environmental Engineering, Yale University, New Haven CT 06520, USA

[4] Energy Sciences Institute, Yale University, West Haven, CT 06516, USA

[5] Renewable and Sustainable Energy Institute, University of Colorado, Boulder, CO 80309, USA

[6] Materials Science Center, National Renewable Energy Laboratory, Golden, CO 80401, USA

[7] Department of Physics, University of Colorado Boulder, CO 80309, USA

[8] Department of Chemical and Biological Engineering, University of Colorado, Boulder, CO 80309, USA

[9] These authors contributed equally: Zhenghong Dai, Shuai You

[*]Correspondence: kai.zhu@nrel.gov (K.Z.), nitin_padture@brown.edu (N.P.P.)

For: *ACS Energy Letters* (Letter)

Manuscript No. nz-2024-00510y

ABSTRACT

Carbazole-based self-assembled monolayers (SAMs) at the interface between the metal-halide perovskite (MHP) and transparent conducting oxide (TCO) serve the function of hole-transport layer in *p-i-n* "inverted" perovskite solar cells (PSCs). Here we show that the use of an iodine-terminated carbazole-based SAM increases the interfacial mechanical adhesion dramatically (2.6-fold), and that this is responsible for substantial improvements in the interfacial morphology, photocarrier transport, and operational stability. While the improved morphology and optoelectronic properties impart high efficiency (up to 25.39%) to the PSCs, the enhanced adhesion suppresses nucleation and propagation of pores/cracks during PSC operation resulting in the retention of 96.3% of the initial efficiency after 1,000 hours of continuous-illumination testing at maximum power-point. This demonstrates the strong connection between judicious interfacial adhesion toughening and simultaneous enhancement in the efficiency and operational-stability of *p-i-n* PSCs, with broader implications for the reliability and durability of perovskite photovoltaics before they can be commercialized.

ABSTRACT GRAPHIC

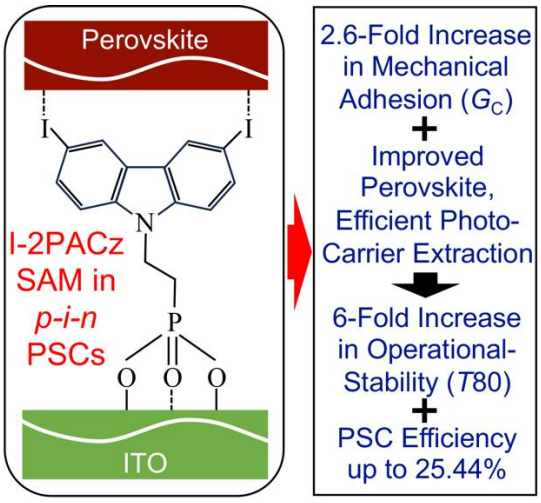

Although single-junction perovskite solar cells (PSCs) [1, 2] have achieved record power-conversion efficiency (PCE) exceeding 26%,[2, 3] critical issues regarding their operational-stability and mechanical reliability need to be addressed before they can be successfully commercialized.[4] In this context, we recently demonstrated a positive correlation between higher interfacial mechanical adhesion toughness and improved operational-stability in rigid [5, 6] and flexible [7, 8] "regular" *n-i-p* PSCs. The premise behind that effort was that stronger mechanical bonding between the various interfaces in a PSC can reduce the propensity for flaw nucleation (pores, cracks) during operation, and enhance the resistance to propagation of any such flaws at those interfaces, thereby preventing delamination.[4] In comparison to *n-i-p* architecture, "inverted" *p-i-n* PSCs show comparable efficiencies but are typically easier to fabricate, have improved stability, and are better suited for tandem photovoltaic (PV) applications. However, the important issue of mechanical adhesion of interfaces in *p-i-n* PSCs has not been addressed adequately. Here we are able to achieve a 2.6-fold increase in the interfacial adhesion toughness *via* judicious selection of SAM, which is much higher than what we were able to achieve in *n-i-p* PSCs (1.5-fold) using a silane-based SAM.[5]

In *p-i-n* PSCs, carbazole-based phosphonic acids that form monolayers or near monolayers (often described as self-assembled monolayers or SAMs) — such as {2-(9*H*-carbazol-9-yl)ethyl}phosphonic acid (2PACz) and {4-(3,6-dimethyl-9*H*-carbazol-9-yl)butyl}phosphonic acid (Me-4PACz) — have recently been used to replace the conventional hole-transporting layer (HTL).[9, 10] Albrecht and coworkers have shown that the carbazole fragment, which has a relatively low ionization energy and a low electron affinity, imparts excellent electron-blocking, and therefore, hole-selective properties to these SAMs.[9] Also, it is well known that the phosphonic acid group binds strongly to the underlying indium-tin oxide (ITO) transparent-conducting oxide (TCO) surface *via* a combination of bi- and tri-dentate bonding.[11] It has been suggested that 2PACz and Me-4PACz SAMs in PSCs provides favorable dipole moments, which contribute towards efficient photocarriers extraction.[9, 10]

Unfortunately, these SAMs are beset with drawbacks such as those associated with the possibility of obtaining incomplete coverage and the reduced wettability of MHP precursor solutions. The coverage issue is being addressed *via* approaches including co-assembly with another SAM;[12] use of an additive;[13] processing approaches;[14] use of ITO surface treatments (UV-O_3,[9] O_2-plasma [15]); use of an oxide layer;[16] and reducing the ITO surface roughness.[17]. Various

strategies for addressing the wettability issue include: introduction of an additive in the SAM-forming molecule solution;[18] use of a porous alumina layer on ITO;[19] incorporation of the SAM-forming molecules in the MHP precursor solution itself where these molecules segregates to the ITO/MHP interface *in situ*;[20] processing approaches;[14] *etc*. Alternatively, wettability can be improved by using methoxy terminal groups on 2PACz-based molecules such as {2-(3,6-dimethoxy-9*H*-carbazol-9-yl)ethyl}phosphonic acid (MeO-2PACz).[9, 10] Most recently, a bi-layer approach has also been used, where an additional molecular "wetting" layer is introduced above the SAM.[21, 22] However, the important issue of how carbazole-based SAMs affects the mechanical adhesion of buried ITO/MHP interface has not been addressed.

In this letter we show that the ITO/MHP interface is quite brittle when the ITO surface is modified by the 2PACz SAM, with an interfacial adhesion toughness, G_C, of 0.49 ± 0.14 J.m^{-2}. To mitigate this issue here we have incorporated the in-house synthesized iodine-terminated 2PACz {2-(3,6-diiodo-9*H*-carbazol-9-yl)ethyl}phosphonic acid (I-2PACz) SAM molecule, which was recently used in organic solar cells,[15] in *p-i-n* PSCs. (Br-2PACz SAM has been used in PSCs recently, but the interfacial mechanical properties are not evaluated in those studies.[14, 22]) This use of I-2PACz SAM in place of 2PACz SAM makes the ITO surface more polar and polarizable for better wettability. Also, the iodine termination provides a favorable dipole. But most importantly, I-2PACz SAM provides dramatically stronger (2.6-fold) mechanical adhesion between ITO and MHP thin film (G_C of 1.29 ± 0.28 J.m^{-2}), thereby reducing microscopic damage to the PSCs during their operation and improving the operational-stability. The use of I-2PACz SAM has resulted in *p-i-n* PSCs with PCE up to 25.39%, and retention of 96.3% of the initial efficiency after 1,000 hours of continuous-illumination testing at maximum power-point (unencapsulated, flowing N_2 atmosphere, ~45 °C).

Figures S1a and S1b in the Supporting Information (SI) compare the contact angle of the MHP precursor solution on glass/ITO substrates with 2PACz or I-2PACz SAMs, respectively; the smaller contact angle in the latter is consistent with better wetting by these polar precursor solutions. MHP thin films (~850 nm thickness) of nominal composition $Cs_{0.05}FA_{0.85}MA_{0.10}Pb(I_{0.97}Br_{0.03})_3$, with 5% excess PbI_2, were solution-deposited on glass/ITO substrates with 2PACz ("control") or I-2PACz ("target") SAMs (see SI for experimental procedures). Figures S2a and S2b present scanning electron microscope (SEM) images of top-surfaces of MHP thin films on 2PACz and I-2PACz SAMs, respectively. The MHP film on I-2PACz

SAM has slightly larger apparent grain size of ~550 nm, compared to ~500 nm in film on 2PACz. Figure S3 presents indexed X-ray diffraction (XRD) patterns of the MHP thin films showing high purity and crystallinity of the α-phase MHP.

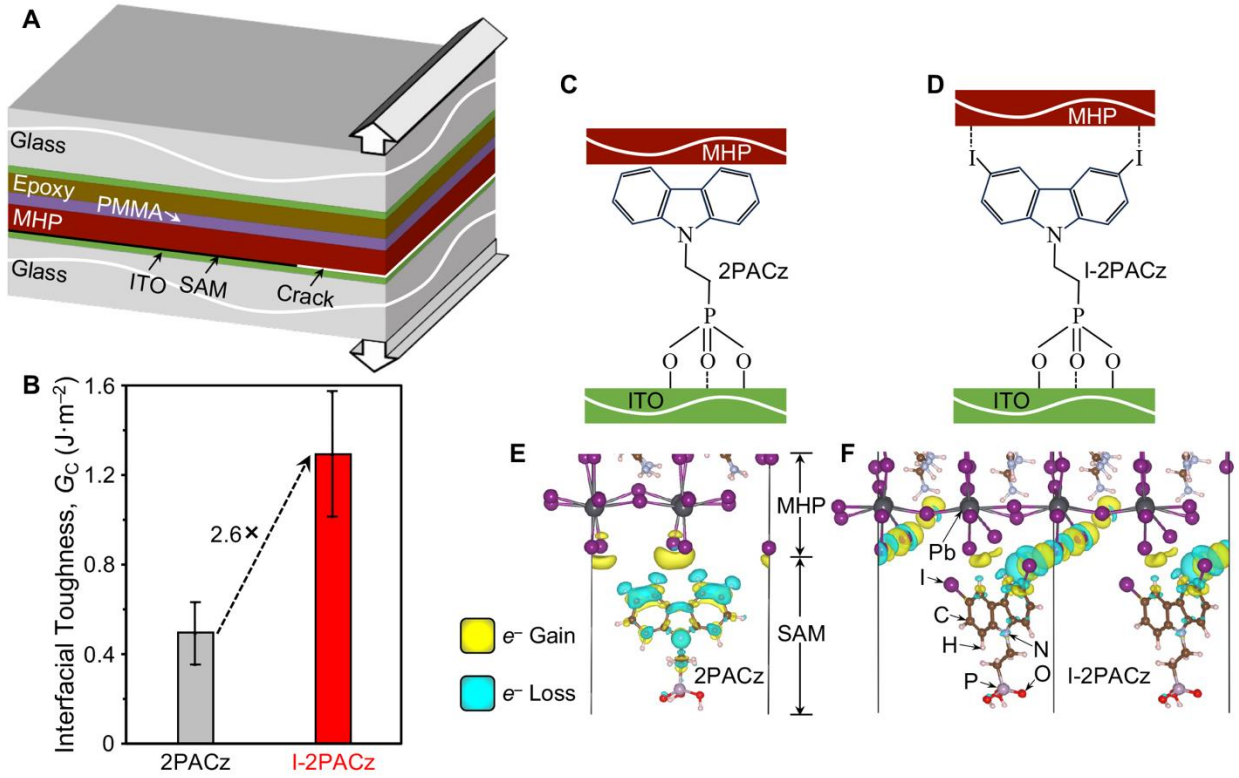

Figure 1. (A) Schematic illustration (not to scale) of the DCB "sandwich" specimen for measuring the interfacial adhesion toughness, G_C. (PMMA = polymethyl methacrylate) (B) G_C of the ITO/MHP interface with 2PACz or I-2PACz SAM at the interface. Average and standard deviation of eight measurements. Schematic illustrations (not to scale) of possible interactions with ITO and MHP of SAM molecules: (C) 2PACz (D) I-2PACz. DFT results showing interactions between I-terminated α-$FAPbI_3$ (001) surface and SAM molecules: (E) 2PACz and (F) I-2PACz.

Figures 1A is a schematic illustration of the double-cantilever beam (DCB) "sandwich" test [5, 23] used to measure the G_C between ITO and MHP, as described in the SI. Figure S4 shows representative examples of measured load-displacement curves. Figure 1B shows a 2.6-fold increase in the measured G_C, from 0.49 ± 0.14 to 1.29 ± 0.28 J.m^{-2}, when a 2PACz SAM interlayer is replaced by an interlayer of I-2PACz SAM. Figures S5a and S5b are SEM images of the delaminated mating fracture surfaces of ITO top side and MHP bottom side, respectively, of interface with the 2PACz SAM interlayer, which indicate clean fracture at the interface. Grain-

boundaries and pores are clearly visible in the MHP bottom side SEM image in the 2PACz case (Fig. S5b). The corresponding SEM images in the case of I-2PACz in Figs. S5c and S5d show the same clean interfacial fracture and MHP grain boundaries, but no pores are seen on the MHP bottom side (Fig. S5d), attesting to the improved quality of the MHP thin film on I-2PACz SAM.

Figures 1C and 1D are schematic illustrations of the 2PACz and I-2PACz SAM molecules, respectively, that bond to the ITO in the same way; however, stronger bonding of I-2PACz to the MHP is expected (Fig. 1D). The basis for this expectation is our previous study showing stronger bonding between an I-terminated silane-based SAM and a MHP, which directly translates to higher mechanical adhesion toughness.[5] This was attributed to the interaction of the terminal iodo group bonding to undercoordinated Pb in the MHP, and to halogen-bonding between the iodo group and iodide ions (and bromide ions) in the MHP.[5] I-terminated I-2PACz was chosen over other halogens in the present study because halogen-bond donor strength of haloorganics follow the order I > Br > Cl > F,[5, 24] and it is compared with the control 2PACz with no halogen terminal group.

To understand the nature of the stronger bonding, and hence the higher mechanical adhesion, of the I-2PACz molecule to MHP, density functional theory (DFT) calculations were performed, as described in the SI.[25] Pure α-$FAPbI_3$ is used in the DFT calculations to represent the MHP, which is a reasonable simplification. This is because the adhesion behavior is dominated by the nature of the halogen (X) anion, relative to the nature of the A-site cation, in a $APbX_3$ MHP, and the very small amount (3%) of Br is expected to have a negligible effect on the DFT adhesion calculations. Figures 1E and 1F compare DFT results for I-terminated α-$FAPbI_3$ (001) surface bonding to the functional groups of isolated 2PACz and I-2PACz molecules, respectively. (See Table S1 in the SI for summary of numerical output from the DFT calculations.) The iodo group of the I-2PACZ has an electrophilic region (the C-I σ^*-orbital), whereas the lone pairs on the iodide ions in the I-terminated MHP surface could donate electron density. Accordingly, electron accumulation (yellow) and electron depletion region (cyan) can be distinctly identified in Fig. 1F, which indicates charge transfer in the interface region and the formation of halogen bonds. The I–I separation (3.30 Å) is considerably shorter than twice the van der Waals radius of two I atoms (~3.96 Å),[26] and than the halogen bond between the organic iodine and the iodide ions for example in a 2D MHP (3.93 Å).[27] In contrast, while electron accumulation and depletion regions can be seen for the 2PACz interaction with the MHP in Fig. 1E, the H–I separation (2.91-3.01 Å) is comparable to the sum of van der Waals radii (3.07 Å), suggesting only a weak hydrogen bond, as

would be expected for an aromatic C–H hydrogen bond donor. Assuming a reasonable areal density of ~1.5 mol.nm^{-2}, where each SAM molecule can rotate about the vertical axis and occupy an exclusive close-packed cylinder, the work-of-separation (W_{sep}) for 2PACz and I-2PACz is calculated to be 0.62 J.m^{-2} and 1.29 J.m^{-2}, respectively — a 2.1-fold increase. Note that the DFT calculations assume full coverage of isolated, upright SAM molecules with no particular rotational orientation. In reality, arrays of SAM molecules may interact with each other, and are typically at an angle with the substrate.[28] But since the W_{sep} calculations use the same areal density for both SAMs, and the aim is to calculate the relative differences, these assumptions are reasonable. Results from DFT calculations for an alternative Pb-I-terminated α-FAPbI$_3$ (001) surface are presented in Figs. S6a and S6b, where the overall W_{sep} values are lower and the difference is smaller (Table S1). However, in reality MHP thin films are created on the SAMs-coated substrates, and it is expected that the formation of the more strongly bonded I-terminated α-FAPbI$_3$ (001) surface will be favored insofar as the iodo groups of the SAM are sterically accessible to the iodine ions. Thus, the significantly higher measured G_C in the I-2PACz case is attributed to the relatively stronger bonding of the terminal I group of that SAM to the MHP.

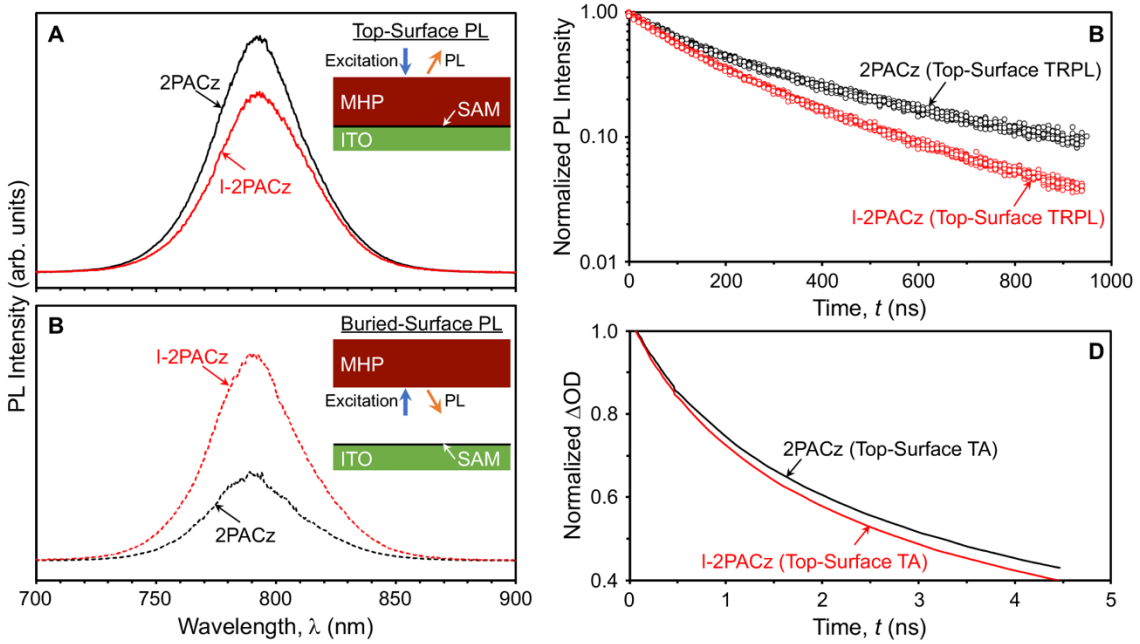

Figure 2. Steady-state PL spectra of MHP thin films on SAMs from: (A) top surface and (B) buried surface after delamination. Insets: schematic illustrations (not to scale) of PL from (A) top MHP surface and (B) buried MHP surface (PMMA/epoxy/ITO above the MHP are not shown). Time-resolved spectra of MHP thin films on SAMs from top surface: (C) TRPL and (D) TA.

Figures 2A presents steady-state photoluminescence (PL) spectra from the top surface of the MHP thin film with 2PACz or I-2PACz SAM underneath. The lower PL intensity in the I-2PACz case indicates more efficient quenching of holes by that SAM. The corresponding time-resolved PL and transient absorption (TA) results presented in Figs. 2C and 2D, respectively, show more rapid decay in the I-2PACz case. The bi-exponential intensity-decay function was used to fit the TRPL data and the results are summarized in Table S2. Note the ~50% increase in the parameter *a* (coefficient for the fast-decay component) and the ~30% decrease in the τ_2 time-constant when the 2PACz SAM is replaced by the I-2PACz SAM, indicating improved hole quenching in the latter. The PL spectra from the buried MHP surface (no hole quenching by SAMs), created by delamination of the ITO/MHP from the above mechanical testing experiments, in Fig. 2B shows a relatively higher PL intensity in the case of I-2PACz than 2PACz. This indicates better quality of the MHP film deposited on I-2PACz SAM, which could be due to the enhanced wetting of the MHP precursor. There is further room for improvement in the wetting by ensuring better I-2PACz SAM coverage using the strategies mentioned earlier. Taken together, the steady-state and time-resolved spectroscopies results in Fig. 2 indicate overall improved optoelectronic properties of the ITO/MHP interface with I-2PACz SAM.

Figure 3A presents current density (*J*) – voltage (*V*) responses of "champion" PSCs with 2PACz or I-2PACz SAM at the ITO/MHP interface (1-sun; AM 1.5G; 100 mW.cm^{-2}; active area 0.079 cm^2; in air); the rest of the PSC structure is the same, and it is depicted schematically in the inset. (See SI for PSC fabrication procedure.) The PV parameters are presented in Table 1, where the maximum PCE (reverse scan) of PSC with I-2PACz is 25.39%. Both PSCs show slight hysteresis. Figure 3B presents external quantum efficiency (EQE) spectra, with maximum EQE exceeding 92.7%. The J_{SC} from Fig. 3B is 25.06 mA.cm^{-2}, which is comparable to that from the *J-V* response. Figure S7 presents the maximum-power output stability of the corresponding PSCs over 120 s and shows no PCE change. Figures 3C-3F present PV parameter statistics for 20 PSC devices each with 2PACz or I-2PACz SAMs. A significant decrease in the standard deviations, together with an increase in the averages, is observed in all the PV parameters for PSCs with I-2PACz SAMs compared to those with 2PACz SAM. However, the increased V_{OC} is primarily responsible for the increased PCE of the PSCs with I-2PACz SAMs.

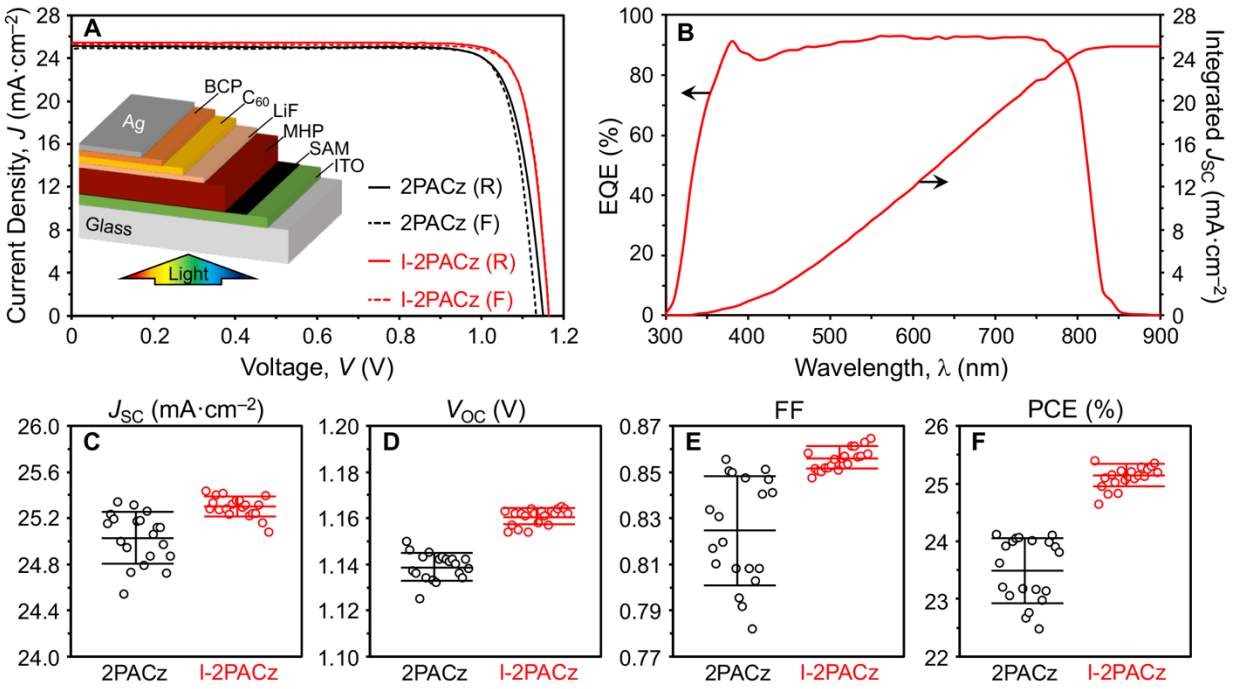

Figure 3. Responses of "champion" PSC with I-2PACz SAM: (A) *J-V* in reverse and forward scans (inset: schematic illustration of the PSC structure (not to scale)) and (B) EQE and integrated J_{SC}. (BCP = bathocuproine) PV parameters (average and standard deviation) of 20 PSCs with 2PACz or I-2PACz SAMs: (C) J_{SC}, (D) V_{OC}, (E) FF, and (F) PCE.

The improved V_{OC} is attributed to the improved electron blocking and/or hole extraction, as indicated by the steady-state PL, TRPL, and TA results in Fig. 2, at the ITO/MHP interface enabled by I-2PACz SAM, and the higher quality of the MHP thin film afforded by the I-2PACz SAM. Also, it has been suggested that halogen termination on a 2PACz SAM can passivate the buried surface of the MHP by filling halide vacancies in the MHP.[14] Furthermore, it has been suggested that a SAM at the ITO/MHP interface with higher positive molecular dipole moment (negative to positive pointing towards ITO) contributes towards increasing the effective work function (ϕ) of the ITO.[9] This may afford a better energy-level alignment with the valence band maximum (VBM) of the MHP, resulting in higher V_{OC} in *p-i-n* PSCs.[9] In this context, the dipole moments of 2PACz and I-2PACz SAM molecules were calculated using DFT (see SI for details), and indeed the dipole moment for I-2PACz was found be much greater (+4.41 D) compared to 2PACz (+1.98 D). (Note that Al-Ashouri *et al.* [9] calculate a dipole moment of +2.0 D for 2PACz.) Also, it was confirmed that the effective ϕ of ITO with I-2PACZ SAM is indeed higher (-5.21 eV)

than that with 2PACz (-4.89 eV) using ultraviolet photoelectron spectroscopy (UPS) measurements (Fig. S8). Note that care was taken to prepare the UPS specimens using exactly the same materials and processes used to prepare the PSCs. Since the VBM of our MHP is -5.40 eV,[29] there is a better energy-level alignment with ITO/I-2PACz substrate for hole transport. The tentative energy-levels schematic diagram for our *p-i-n* PSCs is presented in Fig. S9.

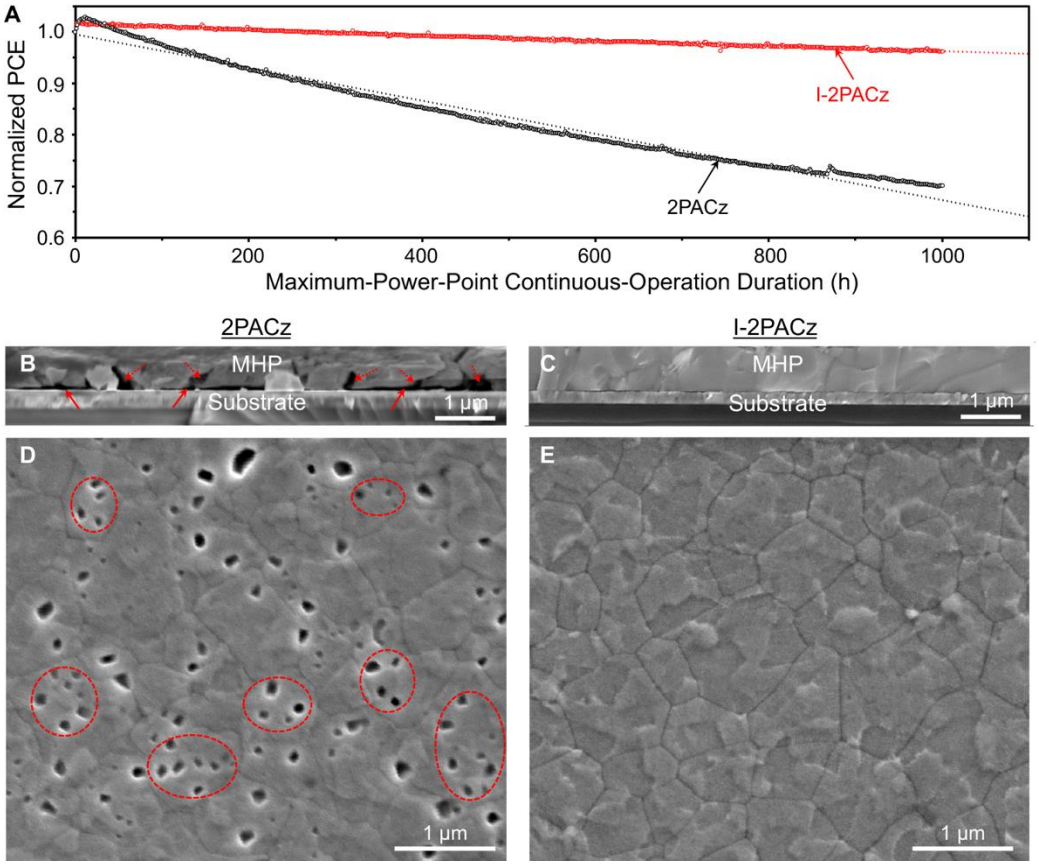

Figure 4. (A) Normalized PCE of PSCs with 2PACz and I-2PACz SAMs as a function of continuous operation duration at 1-sun illumination (unencapsulated; flowing N_2 atmosphere; ~45 °C). Dashed lines are linear fits to the data. Cross-sectional SEM images of 1,000-h-tested PSCs with SAMs: (B) 2PACz and (C) I-2PACz. Dashed and solid arrows in (B) mark pores and delamination, respectively. SEM images of fracture surfaces (MHP side) of 1,000-h-tested PSCs with SAMs: (D) 2PACz and (E) I-2PACz. Dashed ovals in (D) mark some examples of in-grain microscopic pores.

Figure 4A presents operational-stability results for PSCs with 2PACz and I-2PACz under continuous 1-sun illumination with maximum-power-point (MPP) tracking (unencapsulated; flowing N_2 atmosphere; ~45 °C) At the end of 1,000-h testing, the PSCs with 2PACz and I-2PACz SAMs retain 70.0% and 96.3%, respectively, of the initial PCE. The PSC with the 2PACz SAM

shows initial "burn-in," which is not observed in the PSC with the I-2PACz SAM. Thus, linear fits (dashed lines) are used to calculate *T*80 (duration at 80% of the initial PCE retained) employing the extrapolation procedure from the literature,[5, 30] and it is described briefly in the SI. The extrapolated *T*80 for the PSC with 2PACz SAM is estimated at 663 h, whereas the PSC with I-2PACz SAM is considerably more stable (over 6-fold), with an extrapolated *T*80 of 4,062 h.

To understand the longer operational lifetime of PSC with I-2PACz SAM, the 1,000-h-tested PSCs were carefully cross-sectioned and examined in an SEM; Figs. 4B and 4C are cross-sectional SEM images of the ITO/MHP interfaces in the PSCs with 2PACz and I-2PACz SAMs, respectively. The interfacial damage in the PSC with 2PACz SAM is severe and it is characterized by extensive delamination and the presence of microscopic pores. In contrast, the ITO/MHP interface in the 1,000-h-tested PSC with I-2PACz SAM appears almost pristine. This is reflected in the SEM images of the corresponding delaminated fracture surfaces (MHP bottom side) in Figs. 4D and 4E. Figure 4D shows many more pores in the 1,000-h-tested PSC compared to that seen in the initial state that has mostly larger pores (200-400 nm diameter) and only at grain boundaries (Fig. S5b). Such porosity at MHP grain boundaries in buried interfaces in PSCs have been observed previously,[31] but interestingly, Fig. 4D shows smaller pores (50-100 nm) within MHP grains, which are not observed in the initial state. This indicates that the smaller in-grain pores were generated during the PSC operation. In the PSC with I-2PACz SAM, no pores of any kind are observed in the initial state (Fig. S5d) and after operation for 1,000 h (Fig. 4E). Figures S10 and S11 present corresponding XRD patterns and X-ray photoelectron spectra (XPS), respectively, from the fracture surfaces. The XRD pattern shows evidence for PbI_2 in the PSC with 2PACz SAM indicating degradation of the MHP at the interface, but there is little evidence of that in the PSC with I-2PACz SAM. The XPS Pb 4*f* core level peak shift to higher binding energy in the PSC with 2PACz SAM is indicative of the presence of PbI_2,[32] and also δ-$FAPbI_3$.[33] Thus, the I-2PACz SAM allows the deposition of a higher quality MHP thin film to begin with, and the significantly higher adhesion at the ITO/MHP interface resists the nucleation of flaws (pores, cracks), and arrests the propagation of those that may nucleate, during PSC operation. The net result is significantly improved *T*80 lifetime of PSCs with I-2PACz SAM.

In closing, in this letter we have shown that by judicious interfacial engineering using SAMs the mechanical adhesion of the buried ITO/MHP interfaces in *p-i-n* PSCs can be increased dramatically. This results in a substantive improvements in the operational-stability of the PSCs.

The choice of SAM with an appropriate dipole moment also results in the enhancement of optoelectronic properties at the interfaces, and therefore, an improvement of the PSC PCE. While this study focused on the critical ITO/MHP bottom interface in *p-i-n* PSCs, there are vast opportunities for tailoring different types and combinations of SAMs for engineering other important interfaces (*e.g.* MHP/ETL top interface) in *p-i-n* PSCs simultaneously for improved performance. This work indicates that it is possible to align improvements of efficiency, stability, and reliability critical to the success of *p-i-n* PSCs in which improving mechanical adhesion may be decisive. Thus, it is recommended that all three design criteria — mechanical, chemical, and optoelectronic — should be considered in the development of SAMs for *p-i-n* architecture PSCs for single-junction PV, tandem PV, and PV modules of the future.

ASSOCIATED CONTENT

Supporting Information

Supporting information accompanies this paper and it is available.

Experimental section, and results from optical microscopy, SEM, XRD, XPS, UPS, mechanical testing, PV performance testing, and DFT modeling.

AUTHOR INFORMATION

Corresponding Authors

Nitin P. Padture – School of Engineering, Brown University, Providence, RI 02912, USA; Email: nitin_padture@brown.edu

Kai Zhu – Chemistry and Nanoscience Center, National Renewable Energy Laboratory, Golden, CO 80401, USA; Email: kai.zhu@nrel.gov

Authors

Zhenghong Dai – School of Engineering, Brown University, Providence, RI 02912, USA

Shuai You – Chemistry and Nanoscience Center, National Renewable Energy Laboratory, Golden, CO 80401, USA

Dwaipayan Chakraborty – School of Engineering, Brown University, Providence, RI 02912, USA

Shunran Li – Department of Chemical and Environmental Engineering, Yale University, New Haven CT 06520, USA; Energy Sciences Institute, Yale University, West Haven, CT 06516, USA

Yadong Zhang – Renewable and Sustainable Energy Institute, University of Colorado, Boulder, CO 80309, USA
Anush Ranka – School of Engineering, Brown University, Providence, RI 02912, USA
Stephen Barlow – Renewable and Sustainable Energy Institute, University of Colorado, Boulder, CO 80309, USA
Joseph J. Berry – Materials Science Center, National Renewable Energy Laboratory, Golden, CO 80401, USA; Renewable and Sustainable Energy Institute and Department of Physics, University of Colorado, Boulder, CO 80309, USA
Seth R. Marder – Renewable and Sustainable Energy Institute and Department of Chemical and Biological Engineering, University of Colorado, Boulder, CO 80309, USA; Materials Science Center, National Renewable Energy Laboratory, Golden, CO 80401, USA
Peijun Guo – Department of Chemical and Environmental Engineering, Yale University, New Haven CT 06520, USA; Energy Sciences Institute, Yale University, West Haven, CT 06516, USA
Yue Qi – School of Engineering, Brown University, Providence, RI 02912, USA

Notes

The authors declare no competing financial interests.

ACKNOWLEDGEMENTS

The research at Brown University and the National Renewable Energy Laboratory (NREL) was funded by the U.S. Department of Energy (DOE) Office of Energy Efficiency and Renewable Energy (EERE) under the Solar Energy Technology Office (SETO) (Award No. DE-EE0009511). Additional support for research at Brown University was provided by the U.S. Office of Naval Research (ONR) (Grant No. N00014-20-1-2574), and the DFT research was supported by the Center for Synthetic Organic Electrochemistry funded by the U.S. National Science Foundation (NSF) (Grant No. CHE-2002158). Additional support for research at NREL was provided by the U.S. DOE under Contract No. DE-AC36-08GO28308 with Alliance for Sustainable Energy LLC, the Manager and Operator of NREL. The research at Yale University was primarily supported by the U.S. NSF (Grant No. DMR-2313648). I-2PACz was originally synthesized with support from the U.S. ONR as part of a Multidisciplinary University Research Initiative (MURI) (Award No., N00014-21-1-2180). Resynthesis of the material and analysis at University of Colorado were

supported by the U.S. DOE EERE under SETO (Award No. DE-EE0010502). The views expressed in the article do not necessarily represent the views of the DOE or the U.S. Government. The authors thank Jason Tresback (CNS, Harvard University) for the UPS measurements.

REFERENCES

(1) Miyasaka, T. Perovskite Photovoltaics and Optoelectronics: From Fundamentals to Advanced Applications. Wiley-VCH, 2022.

(2) Padture, N. P. The Promise of Metal-Halide-Perovskite Solar Photovoltaics: A Brief Review. *MRS Bulletin* **2023**, *48*, 983-998.

(3) *https://www.nrel.gov/pv/interactive-cell-efficiency.html* (accessed March 15, 2024).

(4) Dai, Z.; Padture, N. P. Challenges and Opportunities for the Mechanical Reliability of Metal-Halide Perovskites and Photovoltaics. *Nature Energy* **2023**, *8*, 1319-1327.

(5) Dai, Z.; Yadavalli, S. K.; Chen, M.; Abbaspourtamijani, A.; Qi, Y.; Padture, N. P. Interfacial Toughening with Self-Assembled Monolayers Enhances Perovskite Solar Cells Reliability. *Science* **2021**, *372*, 618-622.

(6) Yang, I. S.; Dai, Z.; Ranka, A.; Chen, D.; Zhu, K.; Berry, J. J.; Guo, P.; Padture, N. P. Simultaneous Enhancement of Efficiency and Operational-Stability of Mesoscopic Perovskite Solar Cells *via* Interfacial Toughening. *Adv. Mater.* **2024**, *36*, 2308819.

(7) Dong, Q.; Chen, M.; Liu, Y.; Eickemeyer, F. T.; Zhao, W.; Dai, Z.; Yin, Y.; Jiang, C.; Feng, J.; Jin, S.; Liu, S.; Zakeeruddin, S. M.; Grätzel, M.; Padture, N. P.; Shi, Y. Flexible Perovskite Solar Cells with Simultaneously Improved Efficiency, Operational Stability, and Mechanical Reliability. *Joule* **2021**, *5*, 1587-1601.

(8) Dai, Z.; Li, S.; Liu, X.; Chen, M.; Athanasiou, C. E.; Sheldon, B. W.; Gao, H.; Guo, P.; Padture, N. P. Dual-Interface Reinforced Flexible Perovskite Solar Cells for Enhanced Performance and Mechanical Reliability. *Adv. Mater.* **2022**, *34*, 2205301.

(9) Al-Ashouri, A.; Magomedov, A.; Roß, M.; Jost, M.; Talaikis, M.; Chistiakova, G.; Bertram, T.; Marquez, J. A.; Koehnen, E.; Kasparavicius, E.; Levcenco, S.; Gil-Escrig, L.; Hages, C. J.; Schlatmann, R.; Rech, B.; Malinauskas, T.; Unold, T.; Kaufmann, C. A.; Korte, L.; Niaura, G.; Getautis, V.; Albrecht, S. Conformal Monolayer Contacts with Lossless Interfaces for Perovskite Single Junction and Monolithic Tandem Solar Cells. *Energy Environ. Sci.* **2019**, *12*, 3356-3369.

(10) Al-Ashouri, A.; Köhnen, E.; Li, B.; Magomedov, A.; Hempel, H.; Caprioglio, P.; Márquez, J. A.; Vilches, A. B. M.; Kasparavicius, E.; Smith, J. A.; Phung, N.; Menzel, D.; Grischek, M.; Kegelmann, L.; Skroblin, D.; Gollwitzer, C.; Malinauskas, T.; Jošt, M.; Matič, G.; Rech, B.; Schlatmann, R.; Topič, M.; Korte, L.; Abate, A.; Stannowski, B.; Neher, D.; Stolterfoht, M.; Unold, T.; Getautis, V.; Albrecht, S. Monolithic Perovskite/Silicon Tandem Solar Cell with >29% Efficiency by Enhanced Hole Extraction. *Science* **2020**, *370* (6522), 1300-1309.

(11) Hotchkiss, P. J.; Jones, S. C.; Paniagua, S. A.; Sharma, A.; Kippelen, B.; Armstrong, N. R.; Marder, S. R. The Modification of Indium Tin Oxide with Phosphonic Acids: Mechanism of Binding, Tuning of Surface Properties, and Potential for Use in Organic Electronic Applications. *Acc. Chem. Res.* **2012**, *45*, 337-346.

(12) Deng, X.; Qi, F.; Li, F.; Wu, S.; Lin, F. R.; Zhang, Z.; Guan, Z.; Yang, Z.; Lee, C.-S.; Jen, A. K.-Y. Co-assembled Monolayers as Hole-Selective Contact for High-Performance Inverted Perovskite Solar Cells with Optimized Recombination Loss and Long-Term Stability. *Angew. Chem. Intl. Ed.* **2022**, *61*, e202203088.

(13) Park, S. M.; Wei, M.; Lempesis, N.; Yu, W.; Hossain, T.; Agosta, L.; Carnevali, V.; Atapattu, H. R.; Serles, P.; Eickemeyer, F. T.; Shin, H.; Vafaie, M.; Choi, D.; Darabi, K.; Jung, E. D.; Yang, Y.; Kim, D. B.; Zakeeruddin, S. M.; Chen, B.; Amassian, A.; Filleter, T.; Kanatzidis, M. G.; Graham, K. R.; Xiao, L.; Rothlisberger, U.; Grätzel, M.; Sargent, E. H. Low-Loss Contacts on Textured Substrates for Inverted Perovskite Solar Cells. *Nature* **2023**, *684*, 289-294.

(14) Pitaro, M.; Alonso, J. S.; Mario, L. D.; Romero, D. G.; Tran, K.; Zaharia, T.; Johansson, M. B.; Johansson, E. M. J.; Loi, M. A. A Carbazole-Based Self-Assembled Monolayer as the Hole Transport Layer for Efficient and Stable $Cs_{0.25}FA_{0.75}Sn_{0.5}Pb_{0.5}I_3$ Solar Cells. *J. Mater. Chem. A* **2023**, *11*, 11755-11766.

(15) Lin, Y.; Zhang, Y.; Zhang, J.; Marcinskas, M.; Malinauskas, T.; Magomedov, A.; Nugraha, M. I.; Kaltsas, D.; Naphade, D. R.; Harrison, G. T.; El-Labban, A.; Barlow, S.; Wolf, S. D.; Wang, E.; McCulloch, I.; Tsetseris, L.; Getautis, V.; Marder, S. R.; Anthopoulos, T. D. 18.9% Efficient Organic Solar Cells Based on n-Doped Bulk-Heterojunction and Halogen-Substituted Self-Assembled Monolayers as Hole Extracting Interlayers. *Adv. Energy Mater.* **2022**, *12* (45), 2202503.

(16) Phung, N.; Verheijen, M.; Todinova, A.; Datta, K.; Verhage, M.; Al-Ashouri, A.; Köbler, H.; Li, X.; Abate, A.; Albrecht, S.; Creatore, M. Enhanced Self-Assembled Monolayer Surface Coverage by ALD NiO in p-i-n Perovskite Solar Cells. *ACS Appl. Mater. Interf.* **2022**, *14*, 2166-2176.

(17) Chockalingam, M.; Darwish, N.; LeSaux, G.; Gooding, J. J. Importance of the Indium Tin Oxide Substrate on the Quality of Self-Assembled Monolayers Formed from Organophosphonic Acids. *Langmuir* **2011**, *27*, 2545-2552.

(18) Al-Ashouri, A.; Marčinskas, M.; Kasparavičius, E.; Malinauskas, T.; Palmstrom, A.; Getautis, V.; Albrecht, S.; McGehee, M. D.; Magomedov, A. Wettability Improvement of a Carbazole-Based Hole Selective Monolayer for Reproducible Perovskite Solar Cells. *ACS Energy Lett.* **2023**, *8*, 898-900.

(19) Peng, W.; Mao, K.; Cai, F.; Meng, H.; Zhu, Z.; Li, T.; Yuan, S.; Xu, Z.; Feng, X.; Xu, J.; McGehee, M. D.; Xu, J. Reducing Nonradiative Recombination in Perovskite Solar Cells with a Porous Insulator Contact. *Science* **2023**, *379*, 683-690.

(20) Zheng, X.; Li, Z.; Zhang, Y.; Chen, M.; Liu, T.; Xiao, C.; Patel, J. B.; Kucaiuskas, D.; Magomedov, A.; Scheidt, R. A.; Wang, X.; Harvey, S. P.; Dai, Z.; Morales, D.; Pruett, H.; Wieliczka, B. M.; Kirmani, A. R.; Padture, N. P.; Graham, K. R.; Yan, Y.; Nazeeruddin, M. K.; McGehee, M. D.; Zhu, Z.; Luther, J. M. Co-Deposition of Hole-Selective Contact and Absorber for Improving the Processability of Perovskite Solar Cells. *Nature Energy* **2023**, *8*, 462-472.

(21) Zhang, S.; Ye, F.; Wang, X.; Chen, R.; Zhang, H.; Zhan, L.; Jiang, X.; Li, Y.; Ji, X.; Liu, S.; Yu, M.; Yu, F.; Zhang, Y.; Wu, R.; Liu, Z.; Ning, Z.; Neher, D.; Han, L.; Lin, Y.; Tian, H.; Chen, W.; Stolterfoht, M.; Zhang, L.; Zhu, W.-H.; Wu, Y. Minimizing Buried Interfacial Defects for Efficient Inverted Perovskite Solar Cells. *Science* **2023**, *380*, 404-409.

(22) Pitaro, M.; Alonso, J. E. S.; Mario, L. D.; D.G. Romero; Tran, K.; Kardula, J.; Zaharia, T.; Johansson, M. B.; Johansson, E. M. J.; Chiechi, R. C.; Loi, M. A. Tuning the Surface Energy of Hole Transport Layers Based on Carbazole Self-Assembled Monolayers for Highly Efficient Sn/Pb Perovskite Solar Cells. *Adv. Funct. Mater.* **2024**, *in press*, 2306571. DOI: 10.1002/adfm.202306571.

(23) Rolston, N.; Printz, A. D.; Tracy, J. M.; Weerasinghe, H. C.; Vak, D.; Haur, L. J.; Priyadarshi, A.; Mathews, N.; Slotcavage, D. J.; McGehee, M. D.; Kalan, R. E.; Zielinski, K.; Grimm, R.

L.; Tsai, H.; Nie, W.; Mohite, A. D.; Gholipour, S.; Saliba, M.; Grätzel, M.; Dauskardt, R. H. Effect of Cation Composition on the Mechanical Stability of Perovskite Solar Cells. *Adv. Energy Mater.* **2018**, *8*, 1702116.

(24) Cavallo, G.; Metrangolo, P.; Milani, R.; Pilati, T.; Priimagi, A.; Resnati, G.; Terraneo, G. The Haolgen Bond. *Chem. Rev.* **2016**, *116*, 2478-2601.

(25) Kresse, G.; Furthmueller, J. Efficiency of *Ab-initio* Total Energy Calculations for Metals and Semiconductors using a plane-wave basis set. *Computational Materials Science* **1996**, *6*, 15-50.

(26) Rowland, R. S.; Taylor, R. Intermolecular Nonbonded Contact Distances in Organic Crystal Structures: Comparison with Distances Expected from Van der Waals Radii. *J. Phys. Chem.* **1996**, *100*, 7384-7391.

(27) Tremblay, M.-H.; Bacsa, J.; Zhao, B.; Pulvirenti, F.; Barlow, S.; Marder, S. R. Structures of $(4\text{-Y-}C_6H_4CH_2NH_3)_2PbI_4$ {Y = H, F, Cl, Br, I}: Tuning of Hybrid Organic Inorganic Perovskite Structures from Ruddlesden–Popper to Dion–Jacobson Limits. *Chem. Mater.* **2019**, *31*, 6145-6153.

(28) Love, J. C.; Estroff, L. A.; Kriebel, J. K.; Nuzzo, R. G.; Whitesides, G. M. Self-Assembled Monolayers of Thiolates on Metals as a form of Nanotechnology. *Chem. Rev.* **2005**, *105*, 1103-1169.

(29) Zhang, R.; Huang, Z.; Chen, W.; Lyu, B.; Zhang, H.; X. He; Hu, X.; Song, Y.; Choy, W. C. H. A Self-Assembled Vertical-Gradient and Well-Dispersed MXene Structure for Flexible Large-Area Perovskite Modules. *Adv. Funct. Mater.* **2022**, *33*, 2210063.

(30) Khenkin, M. V.; Katz, E. A.; Abate, A.; Bardizza, G.; Berry, J. J.; Brabec, C.; Brunetti, F.; Bulović, V.; Burlingame, Q.; Carlo, A. D.; Cheacharoen, R.; Cheng, Y.-B.; Colsmann, A.; Cros, S.; Domanski, K.; Dusza, M.; Fell, C. J.; Forrest, S. R.; Galagan, Y.; Girolamo, D. D.; Grätzel, M.; Hagfeldt, A.; Hauff, E. v.; Hoppe, H.; Kettle, J.; Köbler, H.; Leite, M. S.; Liu, S.; Loo, Y.-L.; Luther, J. M.; Ma, C.-Q.; Madsen, M.; Manceau, M.; Matheron, M.; McGehee, M.; Meitzner, R.; Nazeeruddin, M. K.; Nogueira, A. F.; Odabaşı, Ç.; Osherov, A.; Park, N.-G.; Reese, M. O.; Rossi, F. D.; Saliba, M.; Schubert, U. S.; Snaith, H. J.; Stranks, S. D.; Tress, W.; Troshin, P. A.; Turkovic, V.; Veenstra, S.; Visoly-Fisher, I.; Walsh, A.; Watson, T.; H. Xie; Yıldırım, R.; Zakeeruddin, S. M.; Zhu, K.; Lira-Cantu, M. Consensus Statement for Stability

Assessment and Reporting for Perovskite Photovoltaics Based on ISOS Procedures. *Nature Energy* **2020**, *5*, 35-49.

(31) Chen, S.; Dai, X.; Xu, S.; Jiao, H.; Zhao, L.; Huang, J. Stabilizing Perovskite-Substrate Interfaces for High-Performance Perovskite Modules. *Science* **2021**, *373* (6557), 902-907.

(32) Zhidkov, I. S.; Boukhvalov, D. W.; Akbulatov, A. F.; Frolova, L. A.; Finkelstein, L. D.; Kukharenko, A. I.; Cholakh, S. O.; Chueh, C.-C.; Troshin, P. A.; Kurmaev, E. Z. XPS spectra as a tool for studying photochemical and thermal degradation in $APbX_3$ hybrid halide perovskites. *Nano Energy* **2021**, *79*, 105421.

(33) Maeng, I.; Lee, S.; Han, E. Q.; Zhang, Y.; Oh, S. J.; Nakamura, M.; Yun, J.-H.; Wang, L.; Kwon, Y.-K.; Jung, M.-C. Unusual Terahertz-Wave Absorptions in δ/α-Mixed-Phase $FAPbI_3$ Single Crystals: Interfacial Phonon Vibration Modes. *npg Asia Mater.* **2021**, *13*, 75.